Mon. Not. R. Astron. Soc. **000**, 1–7 (2013) Printed 18 August 2014 (MN LATEX style file v2.2)

SPACE WARPS: II. Did we beat the lens finding robots in CFHTLS?

Anupreeta More,[1⋆] Aprajita Verma,[2] Phil Marshall,[2,3] Amit Kapadia,[4] Michael Parrish,[4] Chris Snyder,[4] Julianne Wilcox, Elisabeth Baeten, Christine Macmillan, Claude Cornen, Surhud More,[2] Chris Lintott,[1] Robert Simpson,[1] David Miller,[3] Arfon Smith,[3] Edward Paget,[3] Prasenjit Saha,[4] Rafael Kueng,[4] Kelly Borden,[3] Tom Collett, Thomas Jennings, Matthias Tecza,[1] Layne Wright and possibly others

[1] *Kavli Institute IPMU, University of Tokyo, Japan*
[2] *Dept. of Physics, University of Oxford, Keble Road, Oxford, OX1 3RH, UK*
[3] *Kavli Institute for Particle Astrophysics and Cosmology, Stanford University, 452 Lomita Mall, Stanford, CA 94035, USA*
[4] *Adler Planetarium, Chicago, IL, USA*
[5] *Department of Physics, University of Zurich, Switzerland*

to be submitted to MNRAS

ABSTRACT
We present X new strong gravitational lens candidates found in the CFHT Legacy survey by the SPACE WARPS collaboration.

Key words: gravitational lensing – methods: statistical – methods: citizen science

1 INTRODUCTION

Describe various lens finding algorithms and the motivation for this particular project with CFHTLS. Already searched by robots: enables comparison of techniques. Lenses not yet found by robots, detectable by humans?

In Paper I, we describe the SPACE WARPS website, an online system that enables crowd-sourced detection of gravitational lenses. In this paper, we describe our first lens search with SPACE WARPS in the *CFHTLS* data which we refer to as Paper II.

This paper is organised as follows. In Section **??** we give a brief overview of the SPACE WARPS system, focusing on the aspects most relevant to the interpretation of the results of this first lens search. In Section 2 we introduce the *CFHTLS* imaging data and the known lens samples from the *CFHTLS*. In Section **??**, we explain the training sample generated to aid the SPACE WARPS users in the lens search. In Section 5, we present the new lens candidates and our findings. We discuss the implications of our results for future lens searches in Section 6 and draw conclusions in Section 7.

2 DATA

2.1 The CFHT Legacy Survey

The Canada-France-Hawaii Telescope Legacy Survey (CFHTLS) is a photometric survey in five optical bands ($u^*g'r'i'z'$) carried out with the wide-field imager MegaPrime which has a 1 deg^2 field-of-view and a pixel size of 0.186″. The *CFHTLS* WIDE covers a total area of 171 deg^2 on the sky and it consists of four fields W1, W2, W3 and W4. The field W1 has the largest sky coverage of 63.65 deg^2. The fields W2 and W4 have similar sky coverages of 20.32 deg^2 and 20.02 deg^2, respectively[1]. The field W3 has a sky coverage of 42.87 deg^2 and is more than twice as large as W2 and W4.

The *CFHTLS* imaging is very homogeneous and has great image quality. Most of the lensed arcs are much brighter in the g band thus, deep imaging in this band is desirable. The limiting magnitude is 25.47 for the g band which goes the deepest among all of the five bands. The mean seeing in the g band is 0.78″. The zero point to convert flux to AB magnitude for all bands is 30. These char-

⋆ anupreeta.more@ipmu.jp

[1] These numbers are estimated from http://terapix.iap.fr/cplt/table_syn_T0006.html

acteristics make *CFHTLS* ideal to do visual inspection for finding lenses. We use the data from the final T0007 release taken from the Terapix website[2] for this work.

We note that the *CFHTLS* is a niche survey with a unique combination of wide imaging with deep sensitivity. It is a precursor to the ongoing wide imaging surveys such as the DES, KIDS and HSC and planned surveys such as the LSST. Searching for lenses with Space Warps in the *CFHTLS* will teach us important lessons and help prepare us for these larger imaging surveys.

2.2 Known *CFHTLS* lens samples

The *CFHTLS* data has been searched for lenses using semi-automated algorithms, primarily, in the g band which is optimal for finding lenses. Here, we briefly mention the lens samples which were known to the authors prior to the lens search with Space Warps. The work by **?** looks for bluish features around bright XXX galaxies and has found XXX lens candidates at galaxy-scales. The arc finding lens search More et al. (2012) has found 127 lens candidates by looking for arcs in g band alone. This sample has both galaxy and groups scale lens candidates. The **?** is a search for edge-on disk lenses done by selecting the galaxy's profile from the Sextractor's output in the i band and has 18 lens candidates.

For the purpose of transparency, the volunteers participating in Space Warps-*CFHTLS* lens search were made aware of these known lens samples. Images containing the lenses from these lens samples were labelled so in the forum Talk where volunteers have the opportunity to discuss their findings with other volunteers and the science team. XXX some references to Paper I ?

2.3 Image Presentation

Preparation of data: divide survey into overlapping tiles.

Presentation of images. Uniform scales, to build intuition and avoid rescales due to bright objects. Arcsinh stretch, to bring out low SB features. Approximately optimized, how? Examples of images.

We carry out a blind search over the *CFHTLS* fields where we, mainly, use the g-r-i color information to look for signs of lensing. We extract contiguous cutouts of size $81.84''$ (440 pixels). The neighbouring cutouts have an overlapping region of $10''$(54 pixels). If a possible lens candidate is too close to the edge of a cutout, this overlap allows the inspector to get a clearer view of the same candidate in a neighbouring cutout. We note that since the images are shown randomly, a given inspector may not necessarily come across the neighbouring cutout unless the inspector classifies a lot of images. However, this is not a problem since we our user base is extremely large and we get multiple classifications of the same image.

3 TRAINING SAMPLE: SIMULATED LENSES

State the importance

[2] http://terapix.iap.fr/cplt/T0006-doc.pdf

3.1 Methodology

We create two main types of simulated lens sample a) galaxy-scale lenses and b) group or cluster-scale lenses. The galaxy-scale lenses are further divided into two types based on the nature of the background sources, namely, galaxies and quasars. Below, we describe how each type of the lens sample was generated.

3.1.1 Galaxy-scale lenses

The $N_{\rm src}$ behind a lens is then calculated by doing the following integral,

$$N_{\rm src} = N_{\rm src}(> L_s, z_s) \int_{z_l}^{\infty} \sigma_{\rm lens}(\sigma, z_l, z_s, q) D_s^2 (1+z_s)^2 \frac{{\rm d}\chi}{{\rm d}z_s} {\rm d}z_s \tag{1}$$

$$N_{\rm src}(> L_s, z_s) = \int_{L_{min}}^{\infty} \Phi(L_s, z_s) {\rm d}L_s \tag{2}$$

where $\Phi(L_s, z_s)$ is the source luminosity function per unit comoving volume, q is the projected axis ratio of the lens ellipticity, χ and D_s are the comoving and angular diameter distances to the source,

We use the elliptical galaxy (LRG) catalog from the *CFHTLS* XXX to select all the foreground galaxies (e.g. $z < 1$) that are potential lenses for the simulated sample. We exclude all those galaxies whose positions match with the lensing galaxies from the known *CFHTLS* SL2S lens samples More et al. (2012) within 2 arcsec (XXX check).

First, we calculate the luminosity and velocity dispersion of each potential lensing galaxy using the CFHT Megacam g and r band magnitudes along with the photometric redshift (z_l) from the LRG catalog. The Megacam magnitudes are converted to SDSS magnitudes[3] and are further k-corrected to redshift $z = 0.1$ (Frei & Gunn 1994). We assume that the evolution of galaxy luminosities is similar to that determined by (Faber et al. 2007), that is, a decline of 1.5 in the m_{r*} from redshift $z = 1$ to $z = 0$ (see Eq. 4).

$$\frac{L}{L_*} = 10.0^{-0.4\ (m_{r\rm SDSS} - m_{r*})} \tag{3}$$

where m_{r*} is

$$m_{r*} = -20.44 + 1.5\ (z_l - 0.1)\,. \tag{4}$$

We use the $L - \sigma$ relation from (**?**) to get the velocity dispersion as given in Eq. 5.

$$\sigma = 142 \left(\frac{L}{L_*}\right)^{1/3} \tag{5}$$

Next, in order to decide whether a galaxy is likely to act as a strong lens, we calculate the lens cross-section ($\sigma_{\rm lens}$) and the number of sources ($N_{\rm src}$) that are in the background. Following (**?**), the lens cross-section is calculated analytically for an isothermal model and is given by

[3] http://www3.cadc-ccda.hia-iha.nrc-cnrc.gc.ca/megapipe/docs/filters.html

Figure 1. Examples of the three types of simulated lenses.

$$\sigma_{\rm lens} = b_I^2 \int_0^{2\pi} 0.5 r^2(\theta) d\theta \tag{6}$$

where b_I is

$$b_I = b_{\rm SIS}\epsilon_3 / sin^{-1}(\epsilon_3)\,, \tag{7}$$

the eccentricity (ϵ_3) is

$$\epsilon_3 = (1 - q_3^2)^{1/2} \tag{8}$$

and the projected axis ratio is given by

$$q_k = \sqrt{q_3^2 \sin^2 i_e + \cos^2 i_e}\,. \tag{9}$$

In the above equations, q_3 is the 3d axis ratio of the ellipsoid and i_e is the inclination angle. Also, $b_{\rm SIS} = 4\pi \frac{c^2}{\sigma^2} \frac{D_s}{D_{ls} D_l}$ and is referred to as the Einstein radius where D_s,D_l and D_{ls} are angular diameter distances to the source, the lens and between the lens and source, respectively.

Next, if the foreground galaxy can act as a lens and has at least one source in the background, then we determine a redshift (z_s) and i-band magnitude of the background source(s). We assume two types of background sources namely, galaxies and quasars. For each source, the redshift and magnitude are generated by drawing randomly from the following redshift and luminosity distributions. For galaxies, we assume the redshift distribution is

$$p_s = \frac{\beta z_s^2 \exp(\frac{z_s}{z_0(m_{\rm lim})})^\beta}{\Gamma(3/\beta) z_0^3(m_{\rm lim})} \tag{10}$$

where $\beta = 3/2$ and $z_0(m_{\rm lim}) = 0.13 m_{\rm lim} - 2.2$ and the luminosity function is

$$n_s = \int_{-\infty}^{m_{\rm lim}} \frac{n_0 {\rm d}m}{\sqrt{10^{2a(m_1 - m)} + 10^{2b(m_1 - m)}}} \tag{11}$$

with parameters $a = 0.30$, $b = 0.56$, $m_1 = 20$ and $n_0 = 3 \times 10^3\ deg^{-2}$ as given in (Faure et al. 2009) and references therein. For quasars, we calculate the luminosity function by following the prescription of (**?**) and use k-corrections by (Richards et al. 2006).

The luminosity function is expressed as

$$\frac{{\rm d}\Phi}{{\rm d}M} = \frac{\Phi_*}{10^{0.4(\alpha+1)(M_{\rm abs} - M_*)} + 10^{0.4(\beta+1)(M_{\rm abs} - M_*)}} \tag{12}$$

where the normalization, $\phi_* = 5.34 \times 10^{-6} h^3$ Mpc^{-3} and break magnitude, $M_* = -20.90 + 5{\rm log}h - 2.5{\rm log}f(z)$. The redshift dependent factor in M_* is given by

$$f(z) = \frac{e^{\zeta z_s}(1 + e^{\xi z_*})}{(\sqrt{e^{\xi z_s}} + \sqrt{e^{\xi z_*}})^2}\,. \tag{13}$$

We adopt the best-fit values $\zeta = 2.98$, $\xi = 4.05$, $z_* = 1.60$ (Oguri & Marshall 2010). For the faint end slope, we use $\beta = -1.45$ whereas for the bright end slope, we use $\alpha = -3.31$ when $z_s < 3$ and $\alpha = -2.58$ at higher redshifts, as prescribed by (Oguri & Marshall 2010). respectively. We note that when calculating $N_{\rm src}$, the source number density is artificially boosted by a factor (see Table 1) to increase the occurrence of simulated lenses. This helps in creating a large enough sample to carry out various performance tests.

Next, we determine properties of the background source for every lens. We follow similar procedures for both background galaxies and quasars. For simplicity, we simulate a single background source behind every lens. In order to select one background source from the $N_{\rm src}$ per lens, we do ray-tracing for all of the $N_{\rm src}$ sources with GRAVLENS (Keeton et al. 2000) and choose sources that satisfy criteria as given below. We determine fluxes of the lensed images and the total magnification of each of the lensed source. We draw a random source for which the flux of the second brightest lensed image and the total magnification of all lensed images are above the thresholds given in Table 1.

Since we want to produce realistic looking lens systems, we simulate lenses in each of the five *CFHTLS* filters. The colors of the background galaxies are drawn randomly from the photometric CFHTLenS catalog (Hildebrandt et al. 2012; Erben et al. 2013). Similarly, we use a quasar catalog from the SDSS Data Release 9 (Pâris et al. 2012) from which colors are drawn to simulate quasar lenses. Next, we assume deVaucoleur's profile to account for the size and shape of the galaxies. The ellipticity and the position angle are drawn randomly between the range given in Table 1. The effective radius of the galaxy is estimated from the Luminosity−size relation (Bernardi et al. 2003) given by

$$R_{\rm eff} = 10^{0.52} \frac{L_r^{2/3}}{(1 + z_s)^2} \tag{14}$$

where $L_r = L_s / 10^{10.2}$. On the other hand, quasars are assumed to follow a Gaussian profile where the σ is equated to that of the median seeing for every filter. The median seeing

values are taken from Table 4 of the official Terapix T0007 release explanatory document [4].

Once all the parameters are determined for the lens and source models, GRAVLENS is used to simulate lensed images. After accounting for the shot noise in the lensed images and convolving them with the median seeing in each of the filters, the simulated image is added to the real *CFHTLS* image centered on the lensing galaxy. Note that we ensure that the lensed galaxies and lensed quasars do not have the same lensing galaxy in the foreground. Similarly, the lensing galaxies from the galaxy-scale lenses are distinct from the central galaxies of groups-scale lenses which are described in the following section.

3.1.2 Groups-scale lenses

At group or cluster-scales, the brightest group galaxy (BGG) at the center alone does not cause strong lensing. We need to account for the extra convergence arising from the dark matter component as well as satellite galaxies, at least, in the inner regions which are typically responsible for the multiple lensed images (**?**Oguri 2006). Owing to the lack of an appropriate group catalog for our purposes, we create a basic group catalog based on the magnitudes and photometric redshifts available for the *CFHTLS*. We select all galaxies with $10^{10.8} M_{\odot}$ as the BGGs. We select the member galaxies such that their photometric redshifts are within $\delta z = 0.01$ of the BGG and within an aperture of 250 Kpc.

We adopt an isothermal ellipsoid for the BGG and members whenever the ellipticities are available else we use an isothermal sphere. On the other hand, we adopt an NFW profile for the underlying dark matter halo. Assuming a constant mass-to-light ratio of 3×0.7 h M_*/L_*, we use the BGG luminosity to estimate the stellar mass. The stellar mass−halo mass relation (**?**), including random scatter, is then used to calculate the halo mass for the lens. Given the halo mass, other key parameters such as the scale radius (r_s) and the density at the scale radius (ρ_s) can be determined for an NFW profile.

As described in Section 3.1.1, we calculate the luminosity and velocity dispersion for the BGG and each of the member galaxies. Next, we calculate the lens cross-section for each potential lensing group. The complexity in the lens models makes it analytically intractable to calculate the size of the caustics[5]. Hence, we use GRAVLENS to determine the area covered by the caustics. We consider only galaxies as our background source population since group or cluster-scale quasar lenses are not expected to be found in the *CFHTLS* (check XXX). Following the same procedure as described in Section 3.1.1, we calculate the number of galaxies expected to lie behind every potential lensing group (see Eq. 1). As before, for each background galaxy within the lens cross-section, a redshift and an i-band magnitude is determined by drawing galaxies randomly from the respective distributions (see Eqs. 10-11).

[4] http://terapix.iap.fr/cplt/T0007/doc/T0007-doc.pdf

[5] The lens mass distribution determines size and shape of the caustics. Any source located within the caustics will form multiple lensed images which is the criteria for strong lensing. To further understand caustics, see XXX.

Table 1. Thresholds used in the selection of the simulated lenses.

Name	gal		qso	
	min	max	min	max
Source Redshift	1.0	4.0	1.0	5.9
Source Magnitude	21.0	25.5	21.0	25.5
boost factor	100 (40†)		1200	
Second brightest image	23		23	
Total magnification	19		20	
Lens shear strength	0.001	0.02	0.001	0.02
Lens shear pa	0	180	0	180
Source ellipticity	0.1	0.6		
Source PA	0	180		

† – corresponds to the factor used for Groups scale lenses.

All those groups that are found to have no background galaxies within the cross-sectional area are rejected and the rest are included as potential lenses. As mentioned earlier, we artificially boost the total number of sources behind every lens but ensure that (check XXX) the statistical properties such as the profile of the image separation distribution are not affected (see Figure 2). We follow the same procedure and apply the same thresholds to determine properties of the lensed galaxies for every lens as are described for galaxy-galaxy lenses in the previous section. The simulated images are added to the real *CFHTLS* images with the BGGs as the center.

3.2 Simulated Lens Sample and Catalog Description

In this section, we describe some of the properties of our simulated sample for each of the three types of lens samples.

The Figure 2 shows Einstein radius distribution for the galaxy-scale (dashed for background quasars and dotted for background galaxies) and groups-scale simulated lenses. For comparison, we show the expected distributions (blue dashed-dotted curves) for an SIS-like density profile at galaxy-scales and an NFW+Hernquist profile at groups-scales. The theoretical curves are taken from (More et al. 2012) wherein the models are explained in detail. We note that the model we adopt at groups-scale also includes SIS or SIE components for the group members unlike the theoretical prediction. The theoretical curves have arbitrary normalizations.

We show the redshift and magnitude distributions of the lensing galaxies in the left and right panels of Figure 3 respectively. Furthermore, we overplot the distributions of respective properties of the SARCS lenses from (More et al. 2012) for comparison with arbitrary normalizations. We note qualitative similarities between the simulated and the real lens samples.

Similarly, we show the ellipticity and the position angle of the simulated lens galaxy population extracted from the T0007 release of the *CFHTLS* catalogs in the left and right panels of Figure 3, respectively. As before, the dashed-dotted (blue) curves show the same distribution for the SARCS lens population with arbitrary normalization (More et al. 2012).

We produce catalogs with lens and source properties for each of the three types of lenses. These catalogs are available XXX. The catalogs typically have lens position, redshift,

magnitudes, Einstein radius, ellipticity (whenever available) and shear (for galaxy-scale lenses only). For the background sources, we provide the offset from the lens center, redshift, magnitudes, total magnification, number of lensed images. Additionally, ellipticity and effective radius when the background sources are galaxies.

4 TRAINING SAMPLE: DUDS AND FALSE POSITIVES

A good training sample consists of a representative set of objects that one wants to find and another set of objects which appear to be from the former set but are of different origin in reality and which one can learn to discard efficiently. Indeed, we wanted to have a good training sample for the Space Warps users so that they can correctly identify the true lens candidates. Hence, in addition to the simulated lenses, we added a sample of duds and false positives to the training sample. Duds are images which have been visually inspected by experts and confirmed to contain no lenses. False positives are systems which look like lenses but are not, for example, spiral galaxies, starforming galaxies, chance alignments of features arranged in a lensing configuration and stars.

We selected a sample of 450 duds for the Stage I classification in Space Warps (see XXX) and a sample of XXX false positives for the Stage II inspection (see XXX). The sample of false positives was selected from the candidates which passed the Stage I of Space Warps. We note that this is the first time, we have a systematically compiled sample of visually inspected false positives by the Space Warps users and categorized by the science team. Such a sample is tremendously helpful for training and understanding performances of various lens finding algorithms (refer james, sherry's paper ? XXX) **TBA data products; make the FP sample available**

5 RESULTS

5.1 Recovery of lenses

Describe which lenses were recovered and explain any cases missed by citizen scientists

5.2 Stage 1 Classification

5.3 Stage 2 Classification

5.4 Comparison with "Expert" Classification

5.5 Discovery of lenses

Describe the newly found lenses and explain for a few cases why they were missed

5.6 *CFHTLS* completeness and purity

Rejection rate. Completeness and purity at P ¿ retirement, P ¿ 95%, and as function of probability P.

Summarize performance at some fiducial threshold: eg P = 95%.

6 DISCUSSION

Differences with robots: what types of lenses are found at Space Warps*?*

Selection function. Missing system.

Further work.

Describe the importance of this kind of study - being able to quantify the completeness of the lens samples - state how this will be used in a future Space Warps *paper*

We looked at the locations of simulated and real lenses from our data those were missed by Space Warps compared to the locations of the lenses that got detected. We do not find any obvious dependency in the rate of detections as a function of the position of a given lens for both simulated and real lens sample. Thus, the completeness of the lens sample is not affected by whether a lens is located close to the border or well within the center (see Figure 4). **TBD: redo the completeness vs posn figure using the final real lens sample**

6.1 Limitations and Caveats of the training sample

The simulated sample has certain limitations due to lack of our understanding of various phenonmena in the Universe and due to uncertainties in various parameters of our model. Here, we describe some of the cases or aspects in which the simulations are known to have failed or seem unrealistic.

The parameters required by various scaling relations and the models primarily depend on the photometry of the galaxies, groups and quasars detected in the survey. For galaxy-scale lenses, the lensing galaxies at higher redshifts or which are fainter have poor photometric measurements. This causes relatively larger uncertainties in its luminosity and velocity dispersion and leads to simulated lenses which look implausible. For example, due to a larger uncertainty in the velocity dispersion of the lensing galaxy, the lensed images may have larger image separation than what is expected given the visual priors from the galaxy.

At group-scales, the photometric and redshift estimates are used when defining the group membership. Therefore, errors in redshift estimates generate galaxy groups with BGG or member galaxies with dissimilar properties. In some cases, low redshift spiral galaxies are incorrectly assigned high redshift. Spiral galaxies are typically less massive and low redshift spiral galaxies are unlikely to act as gravitational lenses. Hence, the resulting simulated lenses are not convincing.

We use single Sersic component to describe the light profiles of background galaxies. This is clearly not the most accurate description for galaxies, especially, star-forming galaxies which form a significant fraction of the lensed galaxy population. Star-forming galaxies have complex structures such as star forming knots, spiral arms, bars and disks.

7 SUMMARY AND CONCLUSIONS

In this paper, we describe the framework and procedure used to generate simulated lens sample for the blind lens search in the *CFHTLS* survey in collaboration with Space Warps.

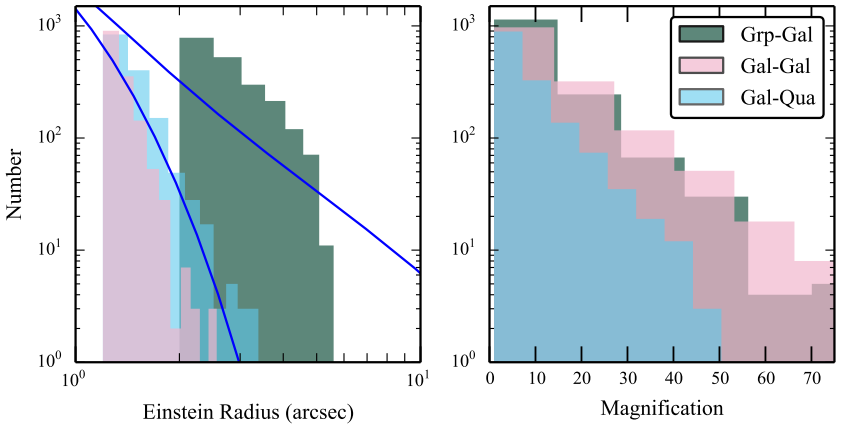

Figure 2. Einstein radius distribution for all types of lenses. The dashed-dotted (blue) curves show the theoretical prediction assuming an SIS model at galaxy-scales and a total (NFW+Hernquist) model at groups-scales taken from (More et al. 2012).

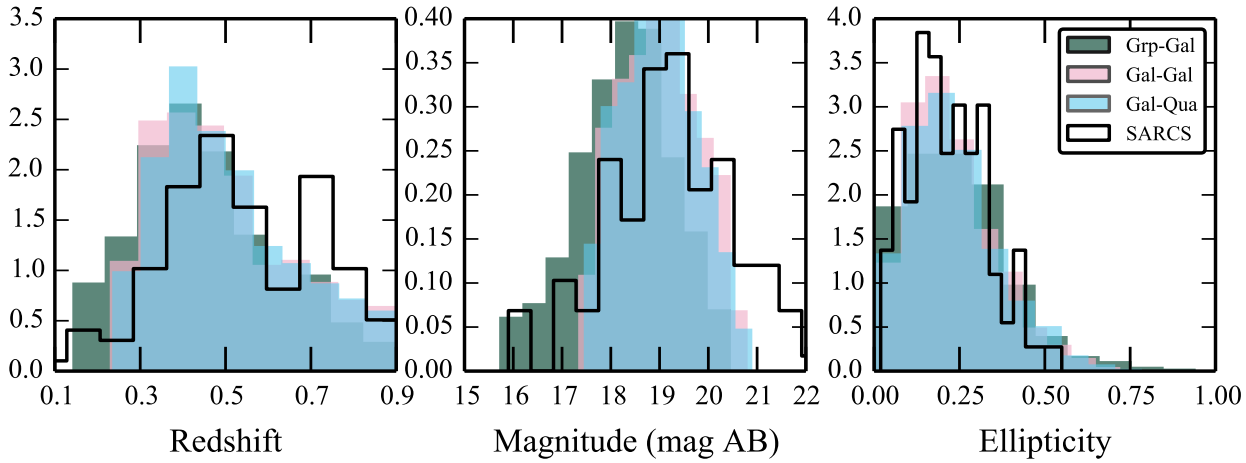

Figure 3. Distributions of properties of the lensing galaxies of the simulated sample compared to the known lens sample SARCS XXXX check?

The aim of this lens search is to find lenses that have been missed by lens finding algorithms. The simulated lens sample is used for training the citizen scientists, calibrating their performance and rejecting unlikely lenses from the sample based on the classifications of citizen scientists. As a result, the simulated lenses need to consist of realistic looking lenses.

We use the photometric and redshift catalogues for the foreground galaxies and additionally, color catalogues for background galaxies and quasars. We use scaling relations to relate light properties to properties such as mass and size to generate lens models. We further account for the instrumental effects such as seeing and noise before creating the final lensed images of model background sources. We add the lensed images on top of the real galaxies and groups in the *CFHTLS* data in all filters.

We draw the following conclusions:

- Crowd-sourced gravitational lens detection works, as shown in by comparing with real lenses in CFHTLS: Real (robotically-detected and expert-confirmed) lenses are recovered/missed at similar/comparable/different rates C% and P% - this is a partial test of supervised vs unsupervised learning
- We found a sample of new gravitational lens candidates. An expert-graded sample of size N, divided among several types. The SW lenses are different from the robotically (RingFinder and ArcFinder) detected lenses, in the following ways.

ACKNOWLEDGEMENTS

We thank all XXXmembers of the Space Warps community for their contributions to the project so far. A complete list of collaborators is given at... In particular we would like to recognise the efforts of XXX, YYY etc in moderating the discussion.

We are also grateful to Brooke Simmons, David Hogg, XXX and YYY for many useful conversations about citizen science and gravitational lens detection. PJM was given support by the Royal Society, in the form

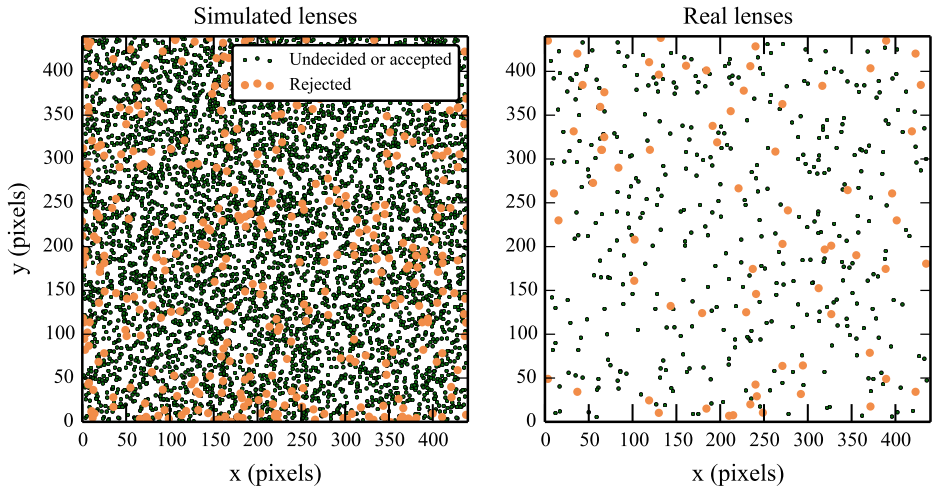

Figure 4. Completeness as a function of location of lenses. Simulated (left) and real lens (right) samples are shown. **: TBD - Add a third color for P> Pthresh which will be defn of "accepted"** Irrespective of whether the lenses are detected or rejected and whether they are simulated or real, there is no obvious dependency on where the lenses are located.

of a research fellowship, and by the U.S. Department of Energy under contract number DE-AC02-76SF00515. The Space Warps project is open source, and was developed at https://github.com/drphilmarshall/SpaceWarps. This work is based on observations obtained with MegaPrime/MegaCam, a joint project of CFHT and CEA/IRFU, at the Canada-France-Hawaii Telescope (CFHT) which is operated by the National Research Council (NRC) of Canada, the Institut National des Sciences de l'Univers of the Centre National de la Recherche Scientifique (CNRS) of France, and the University of Hawaii. This research used the facilities of the Canadian Astronomy Data Centre operated by the National Research Council of Canada with the support of the Canadian Space Agency. CFHTLenS data processing was made possible thanks to significant computing support from the NSERC Research Tools and Instruments grant program. This work was supported by World Premier International Research Center Initiative (WPI Initiative), MEXT, Japan.

This paper has been typeset from a TEX/ LATEX file prepared by the author.

REFERENCES

Bernardi, M., et al. 2003, AJ, 125, 1866
Erben, T., et al. 2013, MNRAS, 433, 2545
Faber, S. M., et al. 2007, ApJ, 665, 265
Faure, C., et al. 2009, ApJ, 695, 1233
Frei, Z., & Gunn, J. E. 1994, AJ, 108, 1476
Hildebrandt, H., et al. 2012, MNRAS, 421, 2355
Keeton, C. R., Christlein, D., & Zabludoff, A. I. 2000, ApJ, 545, 129
More, A., Cabanac, R., More, S., Alard, C., Limousin, M., Kneib, J.-P., Gavazzi, R., & Motta, V. 2012, ApJ, 749, 38
Oguri, M. 2006, MNRAS, 367, 1241
Oguri, M., & Marshall, P. J. 2010, MNRAS, 405, 2579
Pâris, I., et al. 2012, A&A, 548, A66
Richards, G. T., et al. 2006, AJ, 131, 2766